Geophys. J. Int. (1993) **113**, 684–692

A test on the Earth's core–mantle boundary structure with antipodal data: example of Fiji–Tonga earthquakes recorded in Tamanrasset, Algeria

G. Poupinet,[1] A. Souriau[2] and L. Jenatton[1]

[1] *LGIT—Observatoire de Grenoble, BP53X, 38041 Grenoble, France*
[2] *Observatoire Midi-Pyrénées, 14 Avenue Edouard Belin, 31400 Toulouse, France*

Accepted 1992 October 27. Received 1992 October 27; in original form 1992 April 23

SUMMARY

Conflicting models of the core–mantle boundary (CMB) structure have been derived from tomographic inversion of bulletin data: their long wavelength topography ranges from ±3 km to ±7 km according to the model considered. A simple test of these models is provided by the analysis of *PKP(AB)* phases observed at the antipode of a seismic region. Antipodal waves have the peculiarity that they arrive from a wide range of azimuths so that observations at a single station allow us to sample a large volume in the Earth. In particular, *PKP(AB)* samples CMB structure along two circles at 48° distance from the station and from the epicentral region.

We have collected short period and Geoscope seismograms from Fiji–Tonga earthquakes recorded at the antipodal station Tamanrasset, Algeria. The differential traveltime residuals of *PKP(AB)–PKIKP* are analysed as a function of back-azimuth. Their mean value does not vary by more than ±0.4 s, whereas CMB models, including topography and in some cases heterogeneities above CMB, predict azimuthal variations of up to ±0.9 s. Consequently our data favour a small topography of the core–mantle boundary or a compensating effect in traveltimes between CMB topography and heterogeneities in the lowermost mantle.

Key words: CMB, earthquakes, inversion.

INTRODUCTION

The lower part of the mantle, the *D″* region is known to be heterogeneous (Bullen 1963; Dziewonski 1984) and the radius of the core is supposed to vary from place to place (Hide & Horai 1968; Morelli & Dziewonski 1987). The amplitude of the topography of the core–mantle boundary (CMB) is disputed as different studies give conflicting results (Doornbos & Hilton 1989 for example), whereas studies of rays passing above the CMB show clear lateral heterogeneities. All studies of the CMB based on tomographic inversions use the data collected by the International Seismological Centre (ISC), including secondary phases such as *PcP, PKP(AB), PKP(BC)* and *PKKP*. The instruments and the picking procedure of secondary phases in various observatories may be slightly different and this may bias the results. This data set remains quite small compared to *P*-data sets. New data independent from the ISC data base are necessary to assess the reliability of the proposed tomographic models.

Observations of waves focused at the antipodes of a seismic station have been recognized as a powerful tool for investigating global features of the Earth's structure, in particular departures from sphericity and homogeneity (Butler, Brocher & Rial 1986). As for eigenmodes, a single station can provide a global view of the Earth's interior. Moreover, the amplification by focusing of all but direct *PKIKP* waves makes it possible to identify specific phases such as *PKIIKP* reflected from underside the inner core boundary, which are generally difficult to detect at other distances (Rial & Cormier 1980).

There have been very few studies using antipodal records, mainly because of the limited number of station-epicentre pairs with convenient geographic configuration. The only published studies (Rial 1978; Rial & Cormier 1980) are based on the analysis of a New Zealand earthquake recorded at WWSSN stations in Spain and Portugal. Despite a successful modelling of these data with synthetic seismograms, a rather poor resolution has been obtained because long period records were used.

In order to check the properties of the CMB region, we have studied short period records of Fiji–Tonga events at

the antipodal station Tamanrasset in Algeria. Broad-band Geoscope data and data from the International Seismological Centre have also been processed for comparison.

DATA

Short period data

The Tamanrasset station (TAM) in South Algeria (latitude: 22.792°N, longitude: 5.523°E) is located near the antipode of the Fiji–Tonga seismic region, one of the most active seismic regions on Earth. In the period accessible to us (1964–1978), we selected about 110 records with epicentral distances from 170 to 180° (Table 1). Deep earthquakes constitute approximately one half of our data set and they usually give very sharp *P*-wave onsets. The backazimuths sampled by these data are between −10° and 170°. Fig. 1 is a map with the surface projection of the *PKP* rays used in this study. As TAM is not exactly antipodal to Fiji–Tonga events, the western hemisphere is more poorly sampled than the eastern hemisphere.

The station is equipped with a short-period vertical seismometer recording on photographic paper. Fig. 2 gives a few examples of the short-period seismograms used. All of them clearly show the direct *PKIKP* wave [also called *PKP(DF)*] which propagates through the inner core, and the *PKP(AB)* wave, which propagates through the liquid core, after a refraction at critical angle at the CMB. The $PKP^2(AB)$ phase, similar to *PKP(AB)* for the great arc is sometimes observed. Many records also show clear arrivals of unidentified phases between *PKIKP* and *PKP(AB)*. An analysis of their arrival times did not allow an unambiguous interpretation: some of these phases may be *PKIIKP* but other phases are likely generated near the source.

Table 1. Fiji–Tonga earthquakes selected at the short-period station of Tamanrasset, Algeria. The last two columns give the epicentral distance and backazimuth at the station. Origin times and coordinates are from the PDE data of the US Geological Survey distributed on magnetic tapes.

yr	mo	d	h	mn	sec	depth (km)	distance (deg)	backaz. (deg)
1963	3	26	9	48	20.3	48.0	172.442	156.8
1963	3	26	13	25	1.2	40.0	172.224	156.8
1963	5	20	11	38	5.3	68.0	171.388	157.5
1963	7	4	10	58	13.2	158.0	175.429	140.8
1963	7	29	20	14	7.3	39.0	172.174	161.8
1963	8	25	12	18	12.5	565.0	173.332	38.3
1963	9	8	19	50	29.8	550.0	174.678	99.9
1963	10	7	13	14	24.6	550.0	174.769	100.0
1963	11	16	22	43	26.4	33.0	179.311	44.6
1964	7	9	11	22	5.4	43.0	178.765	114.5
1964	9	29	14	0	14.9	29.0	177.607	358.3
1964	11	17	11	3	6.8	549.0	174.975	98.0
1964	12	1	4	53	23.9	232.0	175.916	17.9
1964	12	28	16	16	11.0	611.0	175.215	82.7
1965	1	17	10	43	17.5	568.0	173.256	106.1
1965	2	11	2	33	29.3	174.0	177.963	61.2
1965	3	7	1	43	11.4	60.0	171.893	158.6
1965	3	22	2	44	47.5	51.0	172.439	352.1
1965	4	10	22	32	46.6	543.0	173.570	39.9
1965	5	22	10	31	39.5	578.0	175.734	67.4
1965	6	2	5	12	59.5	538.0	174.873	99.0
1965	8	20	21	21	51.5	79.0	178.412	90.6
1965	11	18	20	0	19.5	420.0	174.942	38.5
1966	3	17	15	50	33.1	639.0	175.304	69.8
1966	6	1	11	47	32.7	22.0	179.232	157.3
1966	7	21	18	30	15.3	592.0	173.687	38.5
1966	8	20	22	55	0.9	37.0	178.512	118.7
1966	8	26	0	51	54.1	83.0	174.534	156.9
1967	1	1	7	5	50.2	40.0	172.340	354.7
1967	2	17	10	10	51.6	19.0	178.829	143.9
1967	3	4	6	16	22.7	227.0	175.589	11.5
1967	6	14	5	6	16.3	11.0	172.363	353.6
1967	9	4	3	51	58.9	231.0	170.344	154.1
1967	10	12	6	35	6.7	636.0	175.304	69.8
1967	11	7	3	49	17.4	43.0	171.985	349.7
1967	11	12	10	36	52.0	34.0	173.943	337.0
1967	12	27	16	22	48.5	33.0	179.425	31.3
1968	1	20	21	21	31.6	349.0	171.589	148.7
1968	3	11	8	26	32.8	112.0	173.386	355.2
1968	5	20	7	13	3.0	22.0	171.187	157.9
1968	5	28	9	6	29.9	33.0	171.355	160.6
1968	5	30	19	42	25.1	42.0	171.369	161.7
1968	7	2	4	30	52.7	53.0	172.426	156.6
1968	7	29	11	11	59.5	33.0	179.419	55.7
1968	8	15	6	50	38.7	188.0	177.121	110.6
1968	8	28	11	50	30.4	36.0	176.716	32.3
1968	9	12	22	44	6.5	635.0	175.309	75.6
1968	9	26	14	37	46.2	251.0	177.012	51.7
1968	10	12	19	17	39.9	607.0	175.575	65.3
1968	12	18	20	3	43.9	367.0	175.869	45.9
1969	10	26	6	38	3.4	127.0	173.362	355.6
1970	10	10	21	59	42.9	33.0	170.394	162.1
1970	10	11	3	16	49.6	33.0	170.418	161.0
1970	11	18	16	43	14.1	570.0	170.388	86.6
1973	1	17	9	44	36.8	251.0	172.319	3.8
1973	2	13	15	22	55.1	541.0	173.513	36.3
1973	7	21	4	19	17.1	411.0	175.213	115.9
1973	8	5	15	47	32.9	33.0	173.314	348.7
1973	12	19	12	55	57.1	246.0	177.111	40.6
1973	12	24	8	14	25.1	121.0	176.243	6.4
1973	12	28	5	31	6.4	549.0	174.780	103.0
1974	3	18	10	56	12.4	27.0	171.985	348.5
1974	7	3	23	25	9.3	33.0	173.502	167.3
1974	8	6	18	38	13.1	48.0	178.788	31.6
1974	10	21	4	12	29.4	602.0	173.766	39.2
1974	11	10	4	25	31.8	33.0	172.093	29.5
1975	1	17	9	30	42.3	153.0	175.112	1.2
1975	5	5	20	28	8.3	90.0	178.360	97.9
1975	10	20	22	25	29.0	33.0	172.897	23.6
1975	11	1	6	14	55.5	424.0	174.642	36.8
1976	1	1	1	29	39.6	59.0	173.522	154.6
1976	1	15	10	9	51.9	33.0	173.578	154.8
1976	3	24	4	46	4.4	33.0	172.281	157.5
1976	3	27	19	42	0.8	59.0	171.537	157.7
1976	4	10	17	12	9.2	560.0	173.626	37.0
1976	7	31	0	46	58.0	20.0	171.851	158.3
1976	9	30	23	34	14.4	32.0	171.957	158.5
1976	11	25	14	6	35.4	442.0	175.538	43.0
1976	12	7	11	15	41.5	46.0	175.669	27.4
1976	12	15	7	10	27.8	79.0	174.507	355.2
1977	1	21	6	11	5.6	604.0	173.984	38.1
1977	3	26	8	19	18.5	93.0	175.782	355.7
1977	6	17	2	29	9.8	690.0	174.802	56.7
1977	8	28	14	11	30.3	44.0	173.286	159.6
1977	9	13	0	21	52.6	33.0	172.577	351.1
1977	10	14	4	55	34.8	33.0	172.803	348.9
1978	1	28	19	36	38.6	102.0	175.947	141.2
1978	3	4	4	46	36.1	33.0	179.037	21.3
1978	6	17	15	11	33.5	33.0	173.938	339.5
1978	7	2	4	1	33.3	25.0	172.475	7.5
1978	7	17	13	26	14.9	292.0	171.999	9.4
1978	8	13	20	53	53.8	599.0	173.836	36.8
1978	8	15	12	37	12.8	33.0	171.586	157.6
1979	1	25	4	8	14.2	14.0	172.374	160.2
1979	6	25	11	1	12.1	42.0	176.946	334.9
1979	8	5	0	53	45.9	181.0	177.217	89.0
1979	11	13	20	43	38.8	32.0	179.141	156.0

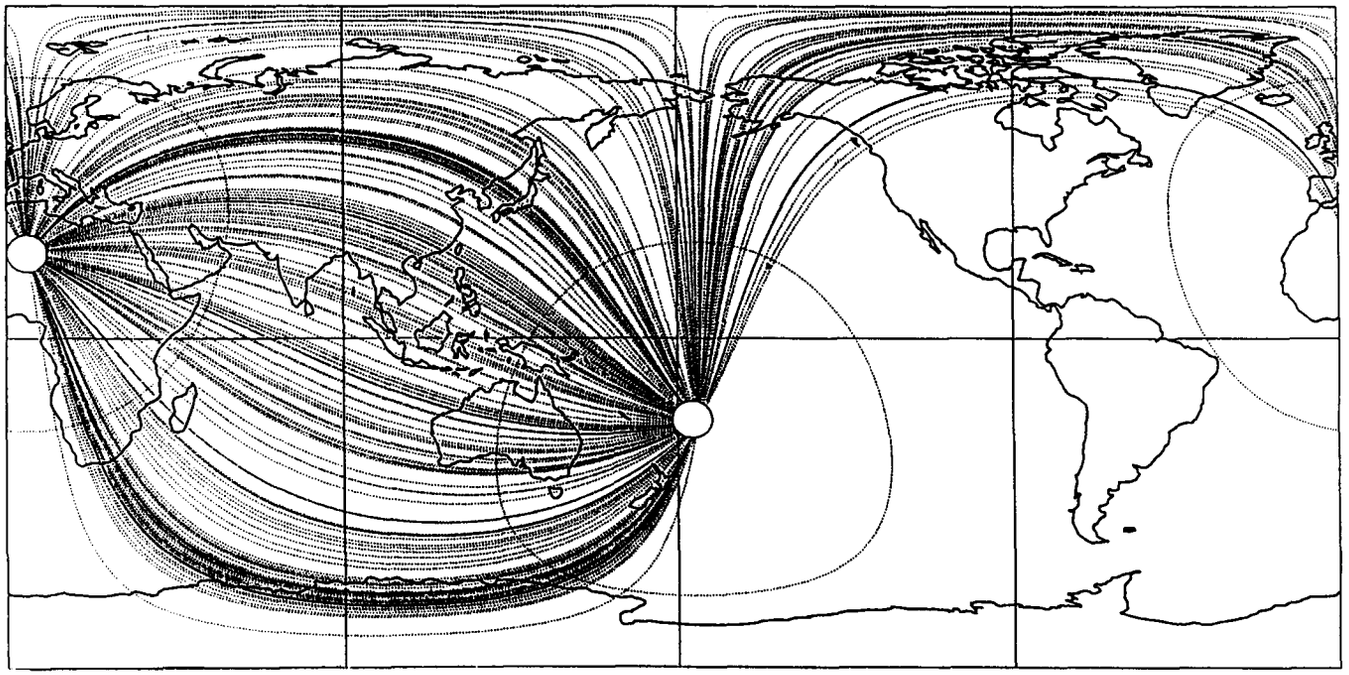

Figure 1. Surface projections of *PKP* rays from the Fiji–Tonga earthquakes used in this study and recorded in Tamanrasset, Algeria. Two circles at a distance of 48° from Tamanrasset and from the barycentre of the epicentres give approximately the points where *PKP(AB)* rays cross the core–mantle boundary.

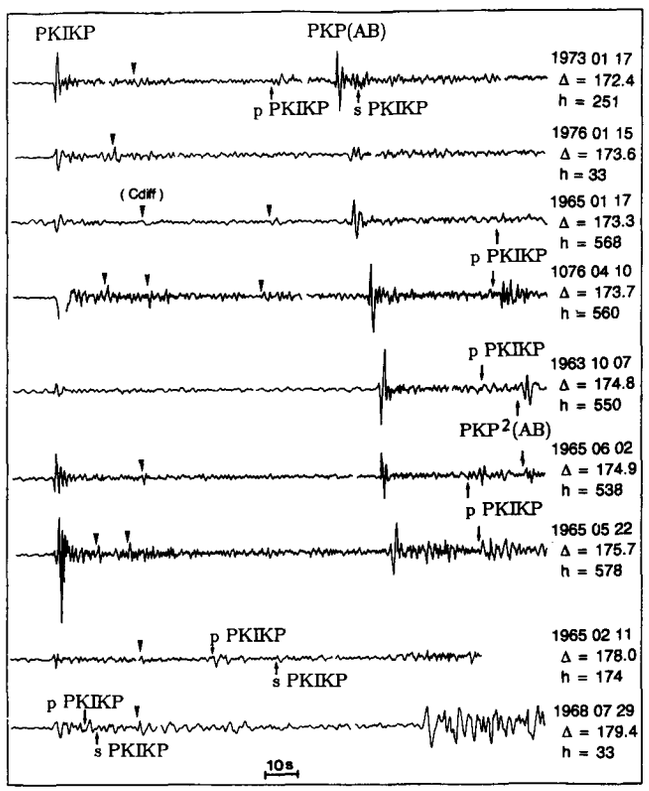

Figure 2. Examples of short-period vertical seismograms of Fiji–Tonga events recorded at Tamanrasset, Algeria. Arrows indicate unknown phases between *PKIKP* and *PKP(AB)*, some of them possibly identified as *PKIIKP*.

GEOSCOPE data

A broad-band station has been installed in Tamanrasset (TAM) since 1989. Five high-quality records of antipodal data have been obtained; two examples are shown on Fig. 3. Accurate differential traveltimes are obtained taking into account the similarity of the waveform of *PKIKP* and of that of the Hilbert transform of *PKP(AB)*. The phase $PKP^2(AB)$ is also easily identified thanks to its waveform similarity to *PKIKP*.

ISC data

Data are available on a CD-ROM for the period 1964–1987. In the epicentral distance range 170 to 180°, only 1180 data are reported with both *PKIKP* and *PKP(AB)* arrival times. Moreover, the distribution of the corresponding direct paths is uneven: the Pacific hemisphere has the best sampling. For station TAM, only 39 data are reported. They are in part a subset of the data we selected, but readings have been made independently.

PKIKP AND *PKP(AB)* TRAVELTIME RESIDUALS

PKIKP and *PKP(AB)* arrival times have been measured on the short-period records at TAM, as well as on the few broad-band Geoscope records available. We have taken into account the fact that the *PKP(AB)* waveform is the Hilbert transform of *PKIKP*. This avoids a systematic time error of a quarter of period. Such an error could be important for the Geoscope data which includes long periods. For a few

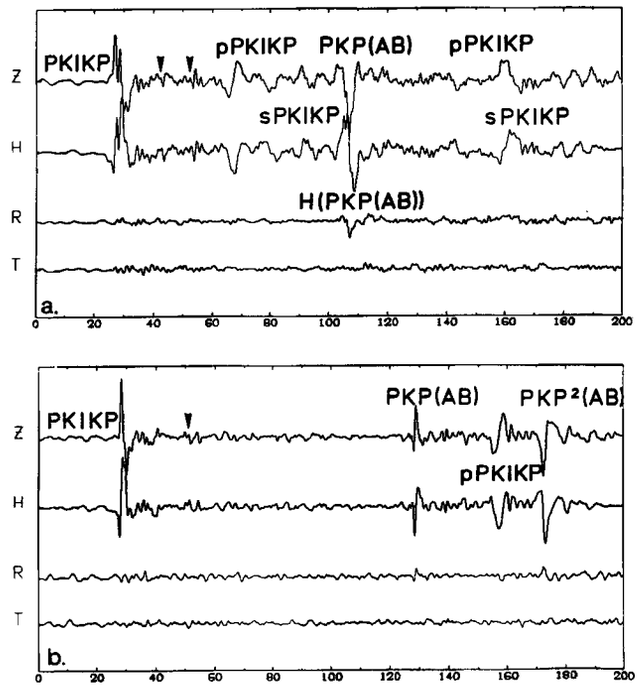

Figure 3. Two examples of broad-band Geoscope records of Fiji–Tonga events obtained at the Tamanrasset, Algeria. *Z, R, T* are respectively the vertical, radial and transverse component and *H* is the Hilbert transform of the vertical component; time is in seconds. (a) 1980 March 21; depth = 145 km, distance = 170.76°, backazimuth = 208°. Note the shape similarity of *PKIKP* with the Hilbert transform of *PKP(AB)*. (b) 1990 July 22; depth = 531 km, distance = 174.9°, backazimuth = 6°. The $PKP^2(AB)$ phase corresponds to *PKP(AB)* travelling along the great arc; its shape is in theory similar to $-PKIKP$. Note the difference in the frequency content of *PKIKP*, *PKP(AB)* and $PKP^2(AB)$, due likely to source directivity. Arrows correspond to onsets possibly identified as *PKIIKP*. *pPKIKP*, *pPKP(AB)*, *sPKIKP* and *sPKP(AB)* are *p* or *s* phases reflected once at the Earth's surface as *p* or *s* and then transmitted as *PKIKP* or *PKP(AB)*.

events, an additional difficulty results from a source directivity effect which induces different frequency contents for *PKIKP* and *PKP(AB)* (see an example in Fig. 3). Most of our data come from short-period analogue records for which the identification of *PKP(AB)* to the *PKIKP* Hilbert transform has been made by eye with help of standard examples. The use of the differential traveltimes of *PKP(AB)–PKIKP* removes clock errors and errors in origin time and depth, but it does not remove errors due to mislocation because of the difference in ray parameters for the two waves considered [close to 0.0–0.4 s/deg for *PKIKP* and close to 4.4 s/deg for *PKP(AB)*]. For each event, the propagation times of the *PKIKP* and *PKP(AB)* phases have been computed for model PREM (Dziewonski & Anderson 1981), an ellipticity correction has been applied (Doornbos 1988) and residuals between observed and computed values have been derived.

There are two ways to compute mean differential residuals between *PKP(AB)* and *PKIKP*. We can either compute separately the average residuals of *PKIKP* and of *PKP(AB)* for various azimuthal ranges and subtract them, or we can compute residuals of *PKP(AB)–PKIKP* differential traveltimes directly and average them per azimuthal range. The data sets differ slightly: differential times are not dependent on clock corrections and can be correct even when the clock of the station drifts. Some *PKIKP* and *PKP(AB)* data can be eliminated because of absolute time problems, but their difference may still be used in the *PKP(AB)–PKIKP* statistics. On the other hand, when a secondary phase is difficult to read, we can use the arrival time of *PKIKP* in our statistics, even if we are unable to read *PKP(AB)*.

Base line corrections

Figure 4 gives the histograms of the *PKIKP*, *PKP(AB)* and *PKP(AB)–PKIKP* residuals at TAM. The histograms of Fig. 4 show that the distribution of the data is symmetrical, except for a few outlyers. In order to exclude the outlyers, we compute the means on a restricted residual range between ±3 s, on both sides of the means. The base line correction is 3.07 s+/−0.15 for *PKIKP*, 4.34 s +/−0.23 for *PKP(AB)* and 1.46 s +/−0.21 for *PKP(AB)–PKIKP*, where the error is one standard deviation.

The baseline correction obtained for *PKP(AB)* is consistent with that of *PREM* (4.22 s, see Table 6(e) in Dziewonski & Anderson 1981). For *PKIKP*, it is higher to the *PREM* one (2.18 s), but similar to that generally obtained for equatorial paths (Poupinet, Pillet & Souriau 1983; Morelli, Dziewonski & Woodhouse 1986; Creager & Jordan 1986; Shearer, Toy & Orcutt 1988; Shearer & Toy 1991; Creager 1992). We have computed for comparison the mean residuals obtained from all the antipodal ISC data corresponding to equatorial or polar paths (Table 2). The mean *PKIKP* residual for equivalent paths is again of the order of 3 s. The station correction of −0.13 s at TAM (Dziewonski & Anderson 1983) indicates that the upper mantle beneath TAM gives a negligible contribution to the residuals of *PKIKP* and *PKP(AB)*. Note from Table 2 that the difference between mean *PKIKP* residuals for polar and equatorial paths based on ISC data reaches 3.5+/−0.6 s, a value much higher than that obtained when all the epicentral distances are considered together (e.g. Poupinet *et al.* 1983). This value is closer to that predicted from eigenmode modelling (Woodhouse, Giardini & Li 1986) and would correspond to a 1.5 per cent uniform anisotropy in the inner core.

Azimuthal residual patterns

Figure 5 shows the residuals and the mean value per azimuthal range as a function of backazimuth in Tamanrasset. Fig. 5(a) corresponds to *PKIKP* residuals shifted by 3.5 s, Fig. 5(b) to *PKP(AB)* residuals shifted by 4.5 s and Fig. 5(c) to *PKP(AB)–PKIKP* residuals shifted by 1.5 s. Different symbols correspond to different types of data and to different depth ranges. We have checked from histograms that, for the different azimuth classes, the distribution of *PKIKP*, *PKP(AB)* and *PKP(AB)–PKIKP* residuals is in most cases symmetrical and close to a Gaussian. Error bars have then been computed from the standard deviation of the distributions. This may be inappropriate when only a few data are available [for example for *PKP(AB)* at mean azimuth 0°].

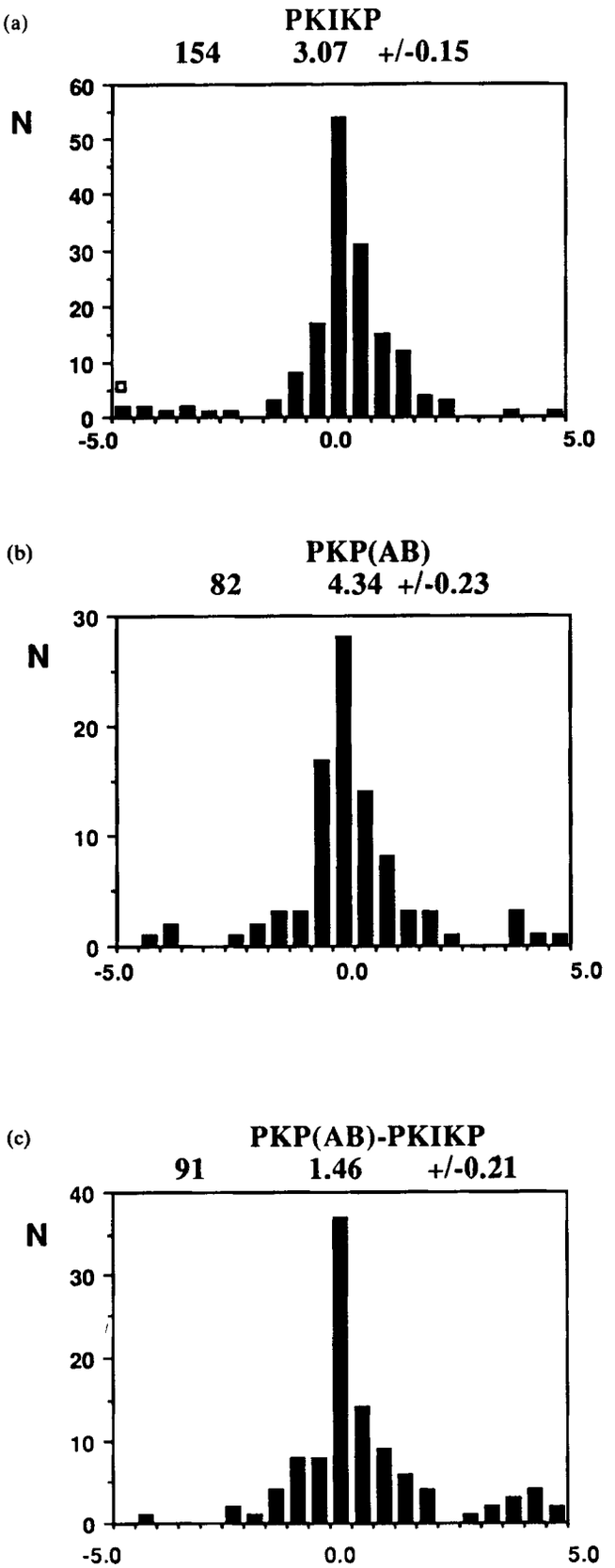

Figure 4. (a) Histogram of *PKIKP* traveltime residuals recorded in Tamanrasset for Fiji–Tonga region. The number of data, mean value and standard deviation of the mean are written on top of the histogram. (b) Histogram for *PKP(AB)* residuals. (c) Histogram for *PKP(AB)–PKIKP*.

Table 2. Mean residual with respect to PREM for nearly diametral rays (epicentral distance: 170°–180°). Equatorial paths: paths located between +/− 30° latitude; polar paths: paths for station/epicentres at latitudes higher than +/−60°. Results obtained from all available ISC data with both *PKP(AB)* and *PKIKP* arrival times. Error bars are one standard deviation.

		Equatorial paths	Polar paths
PKIKP	residual (s.)	3.24 ±0.12	-0.30 ±0.48
PKP(AB)	residual (s.)	4.47 ±0.17	3.77 ±0.29
PKP(AB)-PKIKP	residual (s.)	1.23 ±0.17	4.07 ±0.51
Number of data		169	16

Table 3 and Fig. 6 show that *PKIKP* average mean residual is large for northern azimuths compared to eastern azimuths: the range of residuals goes from 0.66 s for the North to −0.31 s for backazimuth 120°. The residual pattern of *PKP(AB)* is similar to that of *PKIKP*, except for the azimuth 40°. No systematic effect for focal depth is observed. The difference between *PKIKP* and *PKP(AB)* remains close to zero except for 40°, where it reaches −0.42 s. As *PKIKP* and *PKP(AB)* rays are very close to each other in the vicinity of the source, their azimuthal pattern is likely due to the structure in the mantle beneath the sources. The slab in the Fiji–Tonga is dipping towards the West, so that the structure is cylindrical along a nearly N–S axis. For western azimuths in the source region, i.e. eastern backazimuths in TAM, the rays may be affected by the fast velocities in the slab and its downward extension (Inoue *et al.* 1990). It is extremely difficult to correct our data for the residual pattern that may result from a systematic mislocation of the events and from the 3-D velocity distribution in the Fiji–Tonga region.

Table 3 gives the mean residuals of *PKP(AB)–PKIKP*: they vary from −0.30 s to +0.35 s as a function of azimuth. The values of these average differential time residuals are different from the previous estimates using *PKP(AB)* and *PKIKP* separately. However, the estimates of the means remain within the error limits. In any case, both statistics indicate that *PKP(AB)–PKIKP* in TAM for Fiji–Tonga earthquakes do not vary significantly as a function of backazimuth in the interval of azimuth where observations are available.

DISCUSSION

The azimuthal pattern of *PKP(AB)–PKIKP* of Table 3 has to be compared to theoretical computations of azimuthal patterns inferred for tomographic models of *D″* and CMB tomography. The *PKIKP* rays cross the CMB at two nearly antipodal points which do not vary strongly with azimuth. PKP_{AB} crosses the CMB at two points at about 48° from the epicentre and 48° from the station (Fig. 1), so that an azimuthal pattern like in Fig. 5(c) is the sum of the delays on both sides of the CMB. Numerical tests show that a 0.2 s increase in *PKP(AB)* residual can arise from a 2 km change in CMB topography at one of these points or from a 0.3 per cent decrease of the *P* velocity in a 150 km thick *D″* layer above this point. In Fig. 7, we present the theoretical

patterns for three CMB models: Morelli & Dziewonski (1987), Creager & Jordan (1986) and Doornbos & Hilton (1989). *PKP(AB)–PKIKP* azimuthal variations of nearly one second are expected in the azimuth interval of our observations. The data sets used in these models and the inversion procedures are not completely identical. Morelli & Dziewonski (1987) inverted *PcP* and *PKP(BC)* for retrieving CMB topography. Creager & Jordan (1986) used *PKP(AB)* and *PKIKP*, and derived vertical delays at the CMB. Doornbos & Hilton (1989) combined *PcP*, *PKP(AB)*, *PKP(BC)*, *PKKP(BC)* and inverted simultaneously for CMB topography and heterogeneities just above the CMB. In all these experiments, the data have been corrected for the propagation in the upper mantle by removing station corrections, and for the effect of lower mantle heterogeneities given by tomographic models.

Before comparing our results to the values inferred from these tomographic models, it is important to discuss the information contained in *PKP(AB)* data. The size of the Fresnel zone of *PKP(AB)* at the CMB is very large at any epicentral distance: it is close to 20° at a distance of 170° for a wave of period 1 s. Moreover, at about 175°, *PKP(AB)* becomes a diffracted wave. Then this phase is influenced by the structure on a rather large area at the CMB, and it would be strongly distorted if heterogeneities or wavelength of the order of 10° were present in *D″* or at the CMB. It is interesting to note from Fig. 2 that it is not the case: *PKP(AB)* has generally a simple shape, which could be compared to that of *PKIKP*. This suggests that the CMB and the nearby structures do not exhibit strong topography or heterogeneities of short wavelengths. On the other hand, the size of the Fresnel zone of *PKP(AB)* remains small enough (except very close to 180°) so that the tomographic models which are derived, up to degree 4, may be tested from our data. It is worth noting that the CMB tomographic models using *PKP(AB)* data are also affected by a smoothing of the heterogeneities by the large *PKP(AB)* Fresnel zone. Another point to be mentioned is that, contrary to the tomographic models, our data have not been corrected for mantle heterogeneities. The *PKP(AB)* and

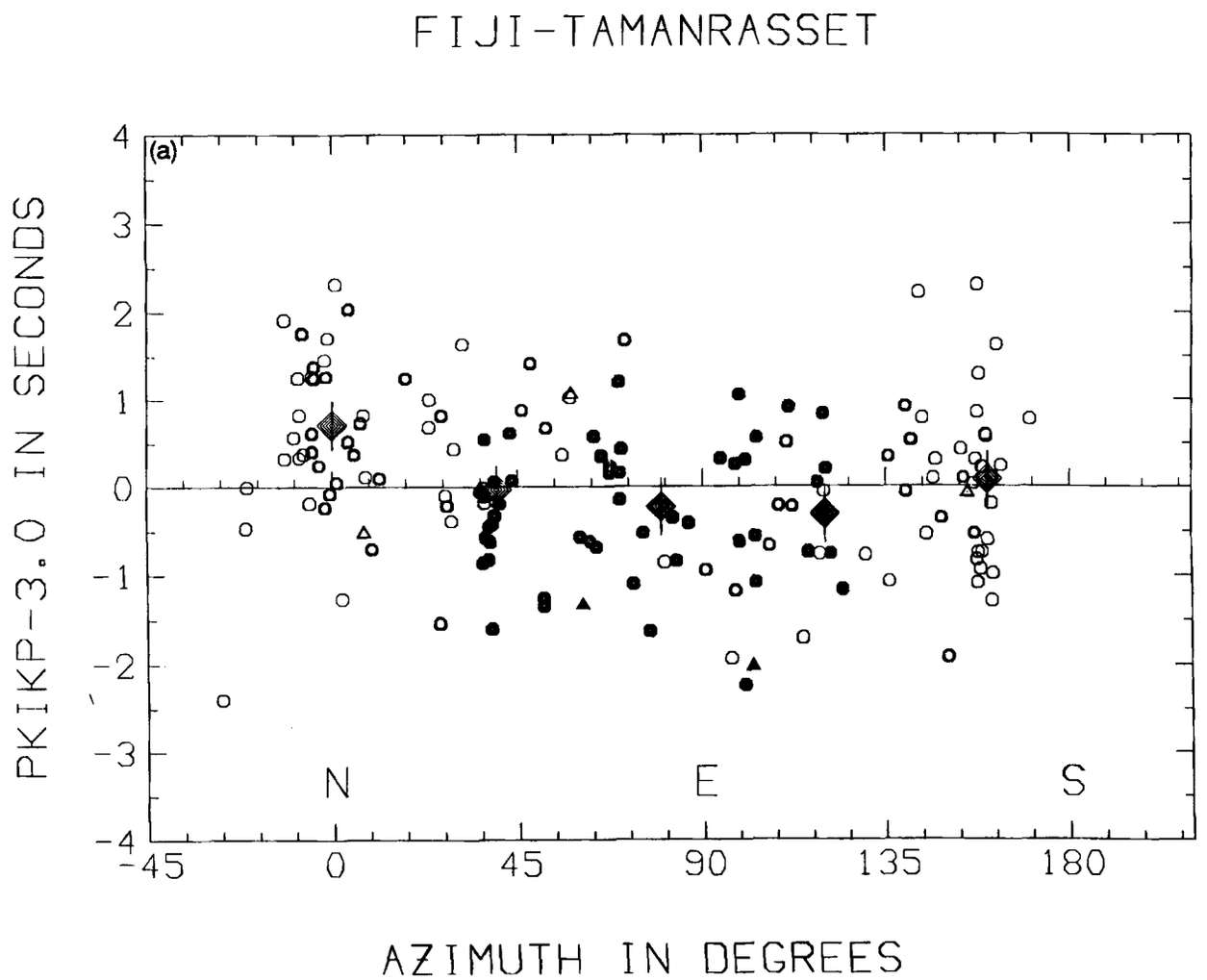

Figure 5. (a) *PKIKP* traveltime residuals for antipodal data at TAM, Algeria, as a function of backazimuth at the station. Residuals are computed with respect to PREM and corrected for ellipticity. Circles are short-period data and triangles are Geoscope data. Thin symbols correspond to events with a depth between 0 km and 70 km, thick symbols with a depth between 70 km and 400 km and full symbols to a depth between 400 km and 700 km. Squares with bars are mean values and standard deviations computed on 40° intervals. A baseline shift of 3.0 seconds is applied to the data. (b) Same as 5(a) for *PKP(AB)* with a baseline shift of 4.5 s. (c) Same as 5(a) for differential times of *PKP(AB)–PKIKP* with a baseline shift of 1.5 s.

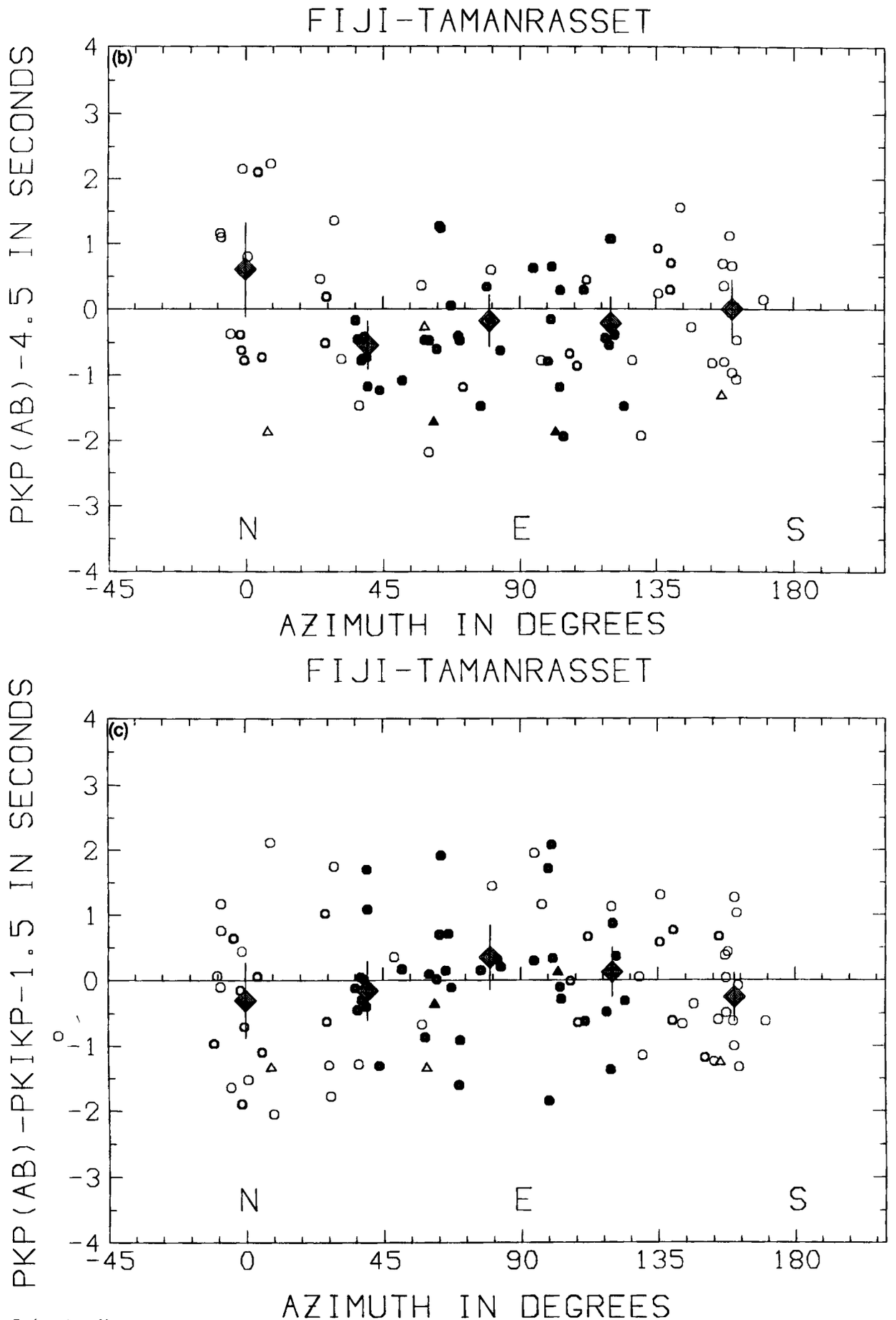

Figure 5. (*continued.*)

Table 3. Statistical analysis of the antipodal data collected in Tamanrasset, Algeria. The azimuthal ranges are listed in column 1. The number of data, the mean residual and the standard deviation are reported for *PKIKP* in column 2, for *PKP(AB)* in column 3, for *PKP(AB)–PKIKP* in column 5. The difference between the mean *PKP(AB)* and the mean *PKIKP* for different azimuthal ranges is in column 4. The distance interval is between 170° and 180°. The residuals and errors are in second.

Back-azimuth	<PKIKP>	<PKP(AB)>	<PKP(AB)> - <PKIKP>	<PKP(AB)> - <PKIKP>
00.0	32	11		16
	0.66	0.61	-0.05	-0.30
	±0.28	±0.72		±0.58
40.0	34	17		19
	-0.03	-0.45	-0.42	-0.15
	±0.30	±0.38		±0.45
80.0	26	16		18
	-0.23	-0.18	0.05	0.36
	±0.33	±0.40		±0.38
120.0	24	21		20
	-0.31	-0.21	0.10	0.13
	±0.33	±0.40		±0.38
160.0	34	13		17
	0.02	0.01	-0.01	-0.26
	±0.32	±0.46		±0.38

PKIKP rays remain close to each other in the upper mantle and in part of the lower mantle (they depart from only 10° at 1700 km depth). Then the azimuthal variations of the *PKP(AB)–PKIKP* data include the effects of the heterogeneities in the lowermost 1000 km of the mantle, in addition to the contribution of the CMB topography. A rough estimate for the L02.56 model by Dziewonski (1984) shows that, if the *D″* layer is excluded, the lowermost mantle does not induce residual variations by more than 0.2 s. Then the observed variations are mainly due to the combined effects of the CMB topography and to *D″* heterogeneities.

Figure 7(a) shows that tomographic models predict *PKP(AB)–PKIKP* azimuthal variations of more than one second in the azimuth interval of our observations. For a comparison with the data, mean values computed inside 40° backazimuth windows have been performed and are reported in Fig. 7(b), together with the observed mean residuals of the differential *PKP(AB)–PKIKP* traveltimes and their 1 σ error bars. Even by applying a systematic

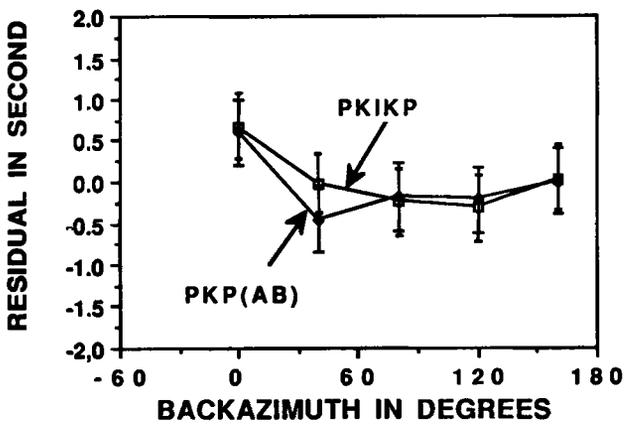

Figure 6. Mean *PKIKP* and *PKP(AB)* as a function of backazimuth in Tamanrasset for Fiji–Tonga earthquakes. Note that the variations of the mean value with backazimuth are very similar except for the azimuth 40°.

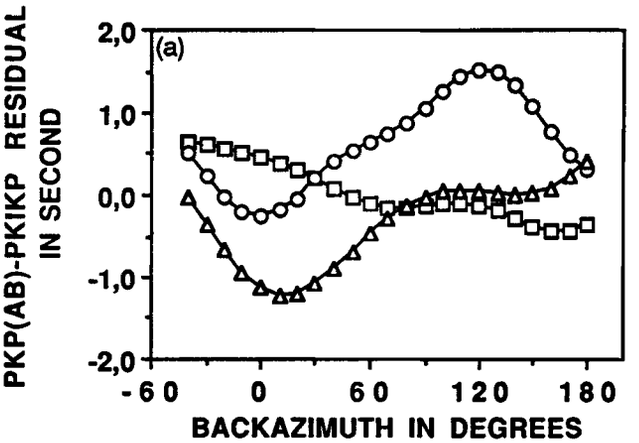

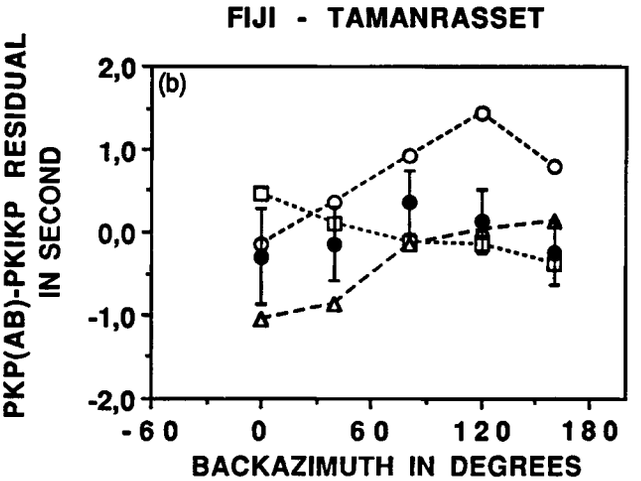

Figure 7. (a) Theoretical *PKP(AB)–PKIKP* azimuthal patterns for the tomographic models of Morelli & Dziewonski (1987) (squares), Creager & Jordan (1986) (circles) and Doornbos & Hilton (1989) including CMB + *D″* heterogeneities (triangles). (b) Mean value of the traveltime residuals of *PKP(AB)–PKIKP* observed in Tamanrasset for Fiji earthquakes as a function of backazimuth. Each solid dot corresponds to the average of the data taken on a 40° backazimuth interval. The 1 σ error bars are reported. The data are compared to the tomographic models presented in Fig. 7(a) (same symbols but averaged on 40° backazimuth intervals).

baseline shift to our data, the models can only fit the observations on a limited azimuth interval. The models by Creager & Jordan (1986) and Doornbos & Hilton (1989), which both include *PKP(AB)* data and take into account *D″* heterogeneities, exhibit an azimuthal dependence similar to that observed in our data in the north-east azimuths, but they slightly overpredict the amplitude of the residuals in the southern azimuths. By contrast, the Morelli & Dziewonski model (1987), which does not take into account *D″* heterogeneities, generates a trend opposite to the observed one and overpredicts the residuals in the northern azimuths. These results suggest that the long wavelength topography of the CMB is compensated in the residual times

by heterogeneities at the base of the mantle or that it remains moderate, with amplitudes not exceeding ±4 km.

This study tested a limited region of the CMB and our conclusions only apply to this region. Nevertheless, it raises questions on the reliability of the tomographic models of the CMB heterogeneities and topography, which are derived from noisy data and explain only a very small part of their variance. Similar antipodal experiments should be attempted to study the details of the core structure.

ACKNOWLEDGMENTS

Funded by 'Action d'accompagnement du projet Geoscope', a project of the French 'Institut National des Sciences de l'Univers' (CNRS). We thank Professor H. Ben Hallou for giving us access to the short-period seismograms at TAM and D. Doornbos for providing us with another set of computations of theoretical residuals for various CMB tomographic models. We also thank A. Pyrolley and F. Besset for their help in retrieving Geoscope data.

REFERENCES

Bullen, K. E., 1963. *An introduction to the theory of seismology,* Cambridge University Press, London.

Butler, R., Brocher, T. M. & Rial, J. A., 1986. Inner core experiments: teleseismic exploration of the antipode, *EOS, Trans Am. geophys. Un.,* **67-8,** 89–94.

Creager, K. C. & Jordan, T. H., 1986. Aspherical structure of the core-mantle boundary from *PKP* travel times, *Geophys. Res. Lett.,* **13,** 1497–1500.

Creager, K. C., 1992. Anisotropy of the inner core from differential travel times of the phases *PKP* and *PKIKP, Nature,* **356,** 309–314.

Doornbos, D. J., 1988. Asphericity and ellipticity corrections, in *Seismological Algorithms—Computational methods and computer programs,* pp. 75–88, ed. Doornbos, D. J., Academic Press, New York.

Doornbos, D. J. & Hilton, T., 1989. Models of core–mantle boundary and the travel times of internally reflected core phases, *J. geophys. Res.* **94,** 15741–15751.

Dziewonski, A. M., 1984. Mapping the lower mantle: determination of lateral heterogeneity in *P* velocity up to degree and order 6, *J. geophys. Res.* **89,** 5929–5952.

Dziewonski, A. M. & Anderson, D. L., 1981. Preliminary reference Earth model, *Phys. Earth planet. Interiors,* **25,** 297–356.

Dziewonski, A. M. & Anderson, D. L., 1983. Travel times and station corrections for *P* waves at teleseismic distances, *J. geophys. Res.* **88,** 3295–3314.

Hide, R. & Horai, K. I., 1968. On the topography of the core–mantle interface, *Phys. Earth planet. Interiors,* **1,** 305–308.

Inoue, H., Fukao, Y., Tanabe, K. Ogata, Y., 1990. Whole mantle *P*-wave travel time tomography, *Phys. Earth planet. Interiors,* **59,** 294–328.

Morelli, A. & Dziewonski, A. M., 1987. Topography of the core–mantle boundary and lateral homogeneity of the liquid core, *Nature,* **325,** 678–683.

Morelli, A., Dziewonski, A. M. & Woodhouse, J. H., 1986. Anisotropy of the inner core inferred from *PKIKP* travel times, *Geophys. Res. Lett.,* **13,** 1545–1548.

Poupinet, G., Pillet, R. & Souriau, A., 1983. Possible heterogeneity of the Earth's core deduced from *PKIKP* travel times, *Nature,* **305,** 204–206.

Rial, J. A., 1978. On the focusing of seismic body waves at the epicentre's antipode, *Geophys. J. R. astr. Soc.,* **55,** 737–743.

Rial, J. A. & Cormier, V. F., 1980. Seismic waves at the epicenter's antipode, *J. geophys. Res.* **85,** 2661–2668.

Shearer, P. M. & Toy, K. M., 1991. *PKP(BC)* versus *PKP(DF)* differential travel times and aspherical structure in the Earth's core, *J. geophys. Res.* **96,** 2233–2247.

Shearer, P. M., Toy, K. M. & Orcutt, J. A., 1988. Axi-symmetric earth models and inner core anisotropy, *Nature,* **333,** 228–232.

Woodhouse, J. H., Giardini, D. & Li, X. D., 1986. Evidence for inner core anisotropy from free oscillations, *Geophys. Res. Lett.,* **13,** 1549–1552.